

# Advancing cost-effective phytochemical cytotoxicity research in cervical cancer through cellular and embryonic studies

Chinmyee Saha<sup>1\*</sup> and Pravin Tirgar<sup>1</sup>

<sup>1</sup>School of Pharmacy, RK University, Rajkot, Gujarat, India

**Abstract.** Cervical carcinoma remains a major contributor to cancer-related morbidity and mortality among women worldwide, with persistent infection by high-risk human papillomavirus (HPV) identified as the principal etiological factor. The present study investigated the anticancer efficacy of six phytoconstituents—quercetin, scopoletin, sulforaphane, icarrin, InUa, and Standard—through combined in vitro and ex vivo approaches. HeLa and SiHa cervical cancer cell lines were treated with graded concentrations (30–100 µg/mL) of each compound, using methotrexate as a pharmacological reference. Cytotoxicity was assessed via viability staining, metabolic assays, and clonogenic survival, all of which demonstrated significant antiproliferative activity and reduced colony formation ( $p < 0.05$ ). Complementary chicken embryo assays substantiated these findings, revealing dose-dependent embryotoxicity. At submaximal doses, quercetin and InUa induced medium turbidity, protein denaturation, necrotic foci, and impaired vascularisation, while higher doses precipitated tissue disintegration, coagulative necrosis, vascular obliteration, and complete embryonic lethality. Sulforaphane, scopoletin, and InUa further caused absolute developmental arrest. Collectively, these results confirm the robust, dose-responsive anticancer and embryotoxic properties of the tested phytochemicals. The findings underscore their translational promise in cervical cancer therapeutics, while highlighting the necessity of precise dose calibration to balance efficacy with biosafety. Future in vivo studies are essential to validate these preliminary observations and refine dosing regimens for clinical application.

---

\*Corresponding author: [csaha320@rku.ac.in](mailto:csaha320@rku.ac.in)

## 1 Introduction

Cervical cancer is a malignant neoplasm originating from the epithelial lining of the cervix and remains one of the leading causes of cancer-related morbidity and mortality among women worldwide. Persistent infection with high-risk human papillomavirus (HPV) is recognized as the primary etiological factor driving disease progression.[1] Cervical carcinogenesis typically advances through cervical intraepithelial neoplasia (CIN), which is classified into three stages: CIN 1 (mild dysplasia), CIN 2 (moderate dysplasia), and CIN 3 (severe dysplasia or carcinoma in situ). The likelihood of progression to invasive carcinoma increases with severity, underscoring the importance of early detection and intervention [1]. Because early stages are often asymptomatic, regular cervical screening using Pap cytology and HPV nucleic acid testing remains essential for timely diagnosis. Several risk factors contribute to the development of cervical cancer, including early sexual debut, multiple sexual partners, chronic tobacco exposure, prolonged use of oral contraceptives, immunosuppression such as human immunodeficiency virus (HIV) infection, and co-infection with other sexually transmitted pathogens [2]. Preventive strategies emphasize prophylactic HPV vaccination, with vaccines such as Gardasil and Cervix demonstrating over 90% efficacy in preventing high-risk HPV infections when administered prior to sexual debut. [2] Complementary public health initiatives, including awareness campaigns and structured screening programs, further enhance early detection and prevention. Therapeutic approaches vary according to disease stage and include surgical procedures (conization, hysterectomy, radical hysterectomy), radiotherapy, and systemic chemotherapy, often applied in combination for advanced disease. Despite these advances, significant global disparities persist. [2] More than 90% of cervical cancer deaths occur in low- and middle-income countries, largely due to limited access to healthcare, screening, and vaccination services [3]. Moreover, while phytochemicals have demonstrated promising anticancer activity, their cost-effectiveness and embryotoxicity profiles remain insufficiently characterized in cervical cancer research.[3] Addressing this gap is critical for developing affordable and safe therapeutic options. The present study investigates the anticancer potential of phytoconstituents—quercetin (*Brassica oleracea*), sulphoraphane (*Brassica oleracea*), scopoletin (*Passiflora incarnata*), inua (*Cichorium intybus*), and icarin (*Epimedium*)—through in vitro assays, including anti-mitotic, brine shrimp lethality (BSL), antimicrobial, germination inhibitory, and 2,2-diphenyl-1-picrylhydrazyl (DPPH) antioxidant tests. Ex vivo chicken embryo studies revealed dose-dependent cytotoxicity, morphological disruption, impaired vascularisation, and complete developmental arrest at higher concentrations, particularly for quercetin, sulphoraphane, and inua. These findings highlight robust antiproliferative and embryotoxic activity, supporting the therapeutic potential of these compounds in cervical cancer management. Future in vivo studies are warranted to validate efficacy and optimise dosing strategies.

## 2 Materials & Methodology

### 2.1 Plant Collection and Identification

*Passiflora incarnata* leaves (Fig. 1.A), *Epimedium sagittatum* roots (Fig. 1.B), *Brassica oleracea* var. *sabellica* (kale) leaves (Fig. 1.C), and *Cichorium intybus* roots (Fig. 1.D) were purchased from Green Earth Products Pvt. Ltd., New Delhi; Ambe NS Agro Products Pvt. Ltd., Ghaziabad, Uttar Pradesh; Yucca Enterprise, Mumbai; and Mirai Organics, Delhi, India, respectively. The plant materials were taxonomically authenticated by Dr. Vaibhavi Savaliya, Professor of Pharmacognosy, School of Pharmacy, R.K. University, Rajkot. Soxhlation, ultrasonication, and maceration extraction processes were employed to obtain

extracts containing the active phytoconstituents quercetin, sulforaphane, scopoletin, inua, and icarrin. Following extraction, chemical confirmatory tests were performed to detect the presence of these phytoconstituents in the extracts.



**Fig. 1.** A-*Passiflora incarnata*, leaves, B-*Epimedium sagittate*, root, C- *Brassica oleracea* var. *sabellica* (Kale), leaves, D- *Cichorium intybus*, roots

### 2.2 Preparation of Methanolic extract of *Berberis vulgaris* by Soxhlet Process

A total of 250 g of dried plant powder was packed into a filter-lined thimble, and methanol extraction was performed at 45 °C for 7–8 hours. The filtrate was concentrated at 40–50 °C and subsequently placed on a water bath, yielding a dark yellow-green semi-solid extract after 2–2.5 hours (Fig. 2.A) [4].



**Fig. 2.** Extraction process by A-Soxhlet process, B) Evaporation process, C) Maceration method

### 2.3. Preparation of UAE

Root powder (100–150 g) was placed in a beaker and immersed in water at threefold volume. Ultrasonic irradiation enhanced extraction at 40–50 °C for 60 min (Fig. 2. B) . The mixture was filtered, and the filtrate was concentrated on a water bath, yielding the aqueous extract [5]

## 2.4. Preparation of ME

Methanol, compatible with *Cichorium intybus* and *Epimedium sagittatum* roots, was added to fully immerse the material. The sealed mixture was macerated for 3–7 days with intermittent agitation, then filtered, and the marc was pressed (Fig. 2.C). The clarified extract was subsequently concentrated by gentle solvent evaporation under reduced temperature [6]

## 2.5. Preliminary Phytochemical Screening- CONFIRMATOY TEST

### 2.5.1. *Passiflora incarnata*

#### A) Coumarins

The sample was dissolved in chloroform, and a few drops of concentrated H<sub>2</sub> SO<sub>4</sub> were added. The solution was mixed thoroughly, and the appearance of a reddish-brown color indicated the presence of sesquiterpene lactones (Fig. 3.A) [7].

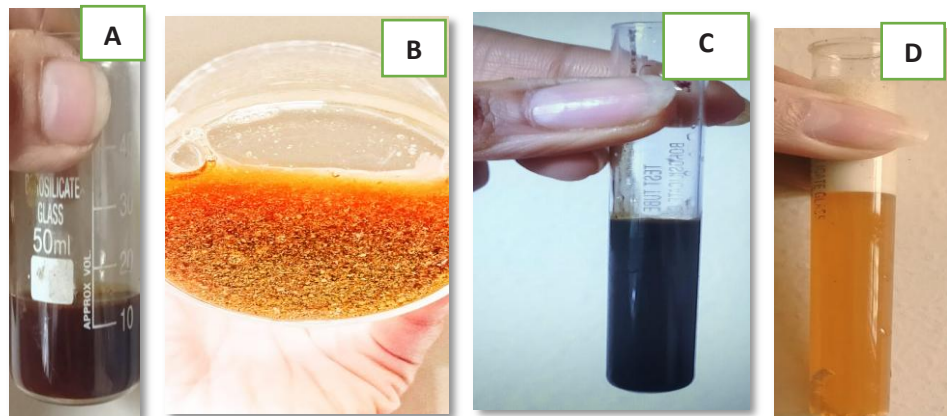


**Fig. 3.A)** Coumarin's test by using chloroform, Flavinioid test, by B) Lead acetate, C) Ferric chloride, D) Shinoda test

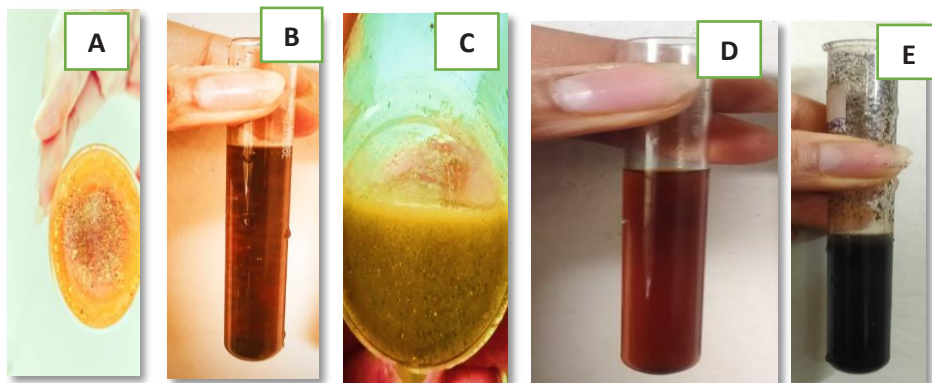


**Fig. 4.** Quercetine test-A) NaoH solution, B) Ammonia solution, Sulphoraphane test by using C) Lead Acetate, Inulin test by using D) Resorcinol & E) Anthrone reagent

### 2.5.2. *Epimedium sagittate*

#### A. Flavinoids:

##### a. Lead Acetate Test:

A few drops of 10% lead acetate solution were added to 1 mL of the alcoholic plant extract. The formation of a yellow precipitate indicated the presence of flavonoids (Fig. 3.B) [8].

##### b. Ferric Chloride:

Added a few drops of 1% ferric chloride solution to 1 mL of an alcoholic extract of the plant. The appearance of a blue color indicates the presence of phenolic compounds, including flavonoids (Fig.3. C) [8]

##### c. Shinoda Test:

A small piece of magnesium or zinc metal was added to 2–3 mL of alcoholic plant extract, followed by the careful addition of a few drops of concentrated hydrochloric acid. The formation of an orange color indicated the presence of flavonoids in the extract (Fig. 3.D) [8].

### 2.5.3. *Brassica oleracea var. sabellica* (Kale)

#### A) Quercetin:

1. The sample extract was treated with 10% NaOH solution. The appearance of a yellow precipitate indicated the presence of quercetin (Fig. 4.A) [9].
2. The sample was treated with HCl and gently heated for a few minutes, followed by the addition of an equal volume of ammonia solution and thorough shaking. The appearance of a red color indicated the presence of quercetin (Fig. 4.B) [9].

### *B) Sulphoraphane:*

The sample extract was mixed with an equal volume of lead acetate solution, and the appearance of a white precipitate indicated the presence of sulforaphane (Fig. 4.C) [10].

#### *2.5.4. Cichorium intybus:*

##### *A) Inulin*

###### *a. Resorcinil Reagent:*

The sample was dissolved in water, and 0.05 g resorcinol was dissolved in 10% concentrated HCl to prepare the reagent. Subsequently, 1 mL of the reagent was added to the sample and heated in a water bath for 5–10 minutes. The appearance of a red color indicated the presence of inulin (Fig. 4.D) [11].

###### *b. Anthrone Test:*

The sample was dissolved in water, and the reagent was prepared by dissolving 0.2% anthrone in 100 mL concentrated sulfuric acid. A few drops of the reagent were added to the sample, which was then boiled in a water bath for 10 minutes. The observation of a greenish-blue color indicated the presence of inulin (Fig. 4.E) [11].

## **2.6. COLONY FORMATION ASSAY**

### *2.6.1. Purposes:*

The clonogenic assay evaluates long-term cell viability and reproductive death following drug or radiation exposure. Unlike short-term cytotoxicity tests, it determines whether surviving cells retain the capacity to proliferate and form colonies. Staining and colony counting enable assessment of treatment impact and IC<sub>50</sub> determination. Initially developed for radiation studies, the assay is now widely applied in chemotherapy research and high-throughput screening to identify selective cytotoxic agents and to evaluate therapeutic efficacy and safety [12].

### *2.6.2. Materials & Preparation:*

HeLa and SiHa cervical cancer cells were cultured in Dulbecco's Modified Eagle Medium (DMEM) supplemented with fetal bovine serum (FBS), antibiotics, and trypsin, and seeded at a density of  $1 \times 10^5$  cells/mL. Phytocompounds were tested at 30, 50, and 100 µg/mL to evaluate dose-dependent effects. Methotrexate (0.1 mg/mL in sterile water) served as the reference drug. Phytocompounds were dissolved in dimethyl sulfoxide (DMSO) to prepare 1 mg/mL stock solutions, filter sterilized (0.22 µm), and diluted into culture medium prior to use. All experiments were conducted under sterile conditions using CO<sub>2</sub> incubators, laminar flow hoods, and multiwell plates. Stained Petri dishes exhibited brownish, purple, and yellow patterns, reflecting treatment-dependent changes in cell viability, cytotoxicity, and metabolic activity [13].

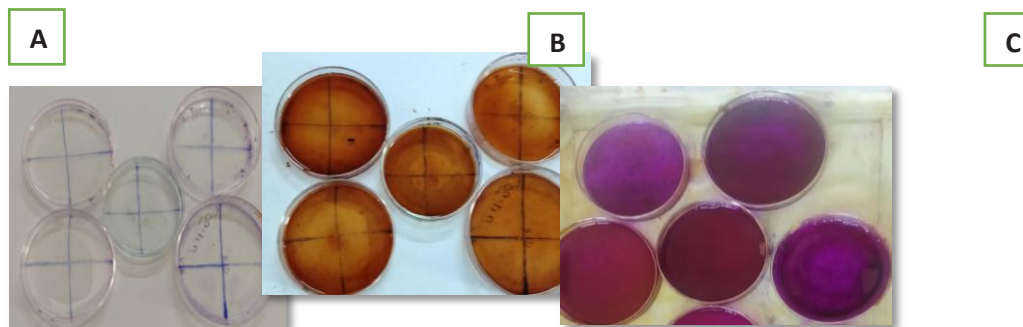


**Fig. 5.** Colony Formation Assay-A) Quartile Area Marking on Petri Plate, B) Cell line & different dosages of test drugs, C) Staining process after treatment for observing microscopic view

### 2.6.3. Process:

HeLa and SiHa cervical cancer cell lines were cultured in complete medium until reaching 70–80% confluency. Cells were harvested using trypsin-EDTA and counted with a hemocytometer. Each sterile 60 mm Petri dish was divided into four equal regions for spatial tracking (Fig. 5.A), and a single test drug—quercetin, sulforaphane, scopoletin, icarin, or inua extract (Fig. 5.B)—was assigned per dish at either 40 or 50  $\mu\text{g}/\text{mL}$  concentration. Stock solutions were prepared in DMSO and diluted in culture medium, while methotrexate was dissolved in sterile water at 0.1  $\text{mg}/\text{mL}$  as a standard control. Cells were seeded evenly across all regions and incubated at 37 °C with 5%  $\text{CO}_2$  for 48 hours. Following incubation, dishes were examined under a phase-contrast microscope, and colony formation was visually assessed after trypan blue staining (Fig. 5.C). The number, size, and density of colonies were recorded to evaluate drug-induced effects on cell proliferation [14–18].

## 2.7. Chicken embryo toxicity assay

### 2.7.1. Purposes:

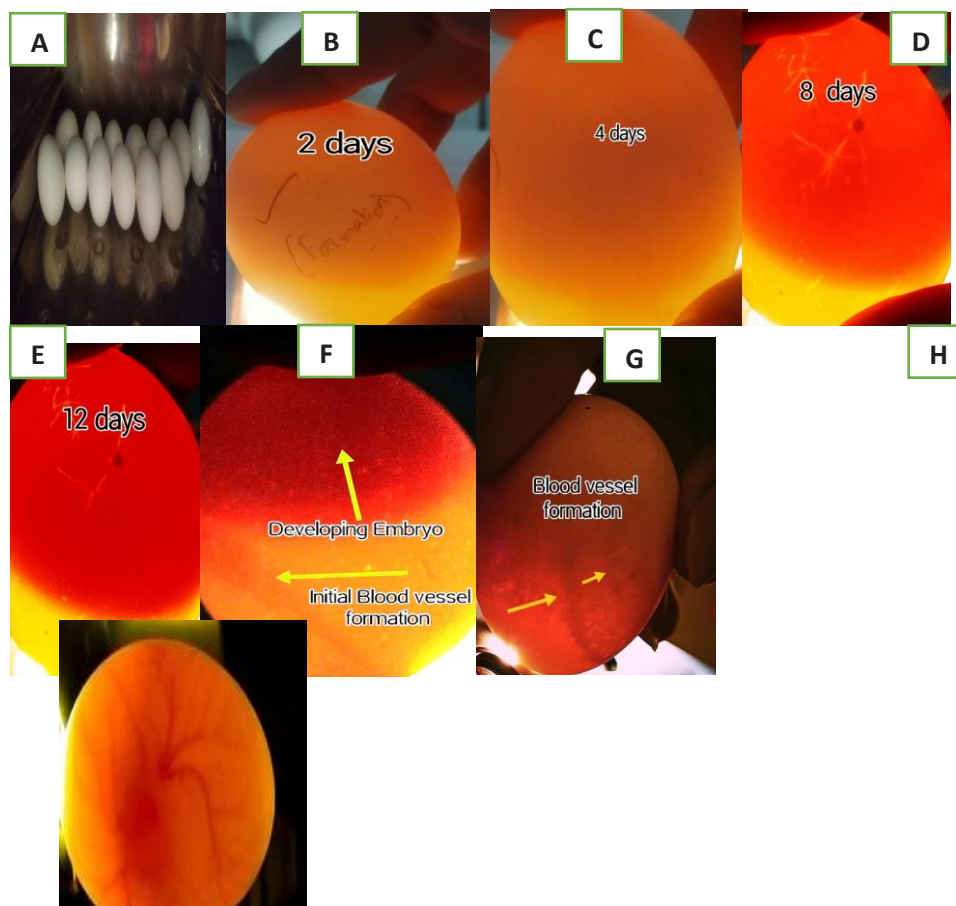
This model enables early assessment of drug toxicity, including embryotoxic and teratogenic effects, prior to mammalian testing. It supports ethical research through the 3R principles and facilitates patient-derived tumor grafts for personalized drug-response prediction. Tumor invasion, metastasis, angiogenesis, and safe dosage ranges can be visualized *in vivo*. In addition, the model allows evaluation of biodistribution and the efficacy of nanoparticle- and liposome-based drug-delivery systems [19].

### 2.7.2. Materials:

Fresh fertilized chicken eggs were employed to evaluate anticancer compounds, including Quercetin, Sulforaphane, Scopoletin, Icarin, and Euxanthone (tested at 30  $\mu\text{g}/\text{mL}$  and 50  $\mu\text{g}/\text{mL}$ ). Methotrexate (0.1  $\text{mg}/\text{mL}$ ) was used as the cytotoxic reference. All compounds were freshly prepared in sterile phosphate-buffered saline (PBS) and stored at 4 °C. The experimental setup consisted of sterile Petri dishes, calibrated micropipettes, dissecting instruments, and a humidity-controlled incubator. Image analysis was performed using ImageJ software [20].

### 2.7.3. Process:

Fresh fertilized chicken eggs were incubated at 37.5 °C with 60–65% humidity for 15 days (Fig. 6.A), with regular rotation to ensure uniform embryonic development. Observations were systematically performed on the 2nd (Fig. 6.B), 4th (Fig. 6.C), 8th (Fig. 6.D), and 12th day (Fig. 6.E) to document embryonic growth and vascular development. The developing embryo was examined (Fig. 6.F), along with partial blood vessel formation (Fig. 6.G) and complete blood vessel formation (Fig. 6.H). On day 15, embryos were observed (Fig. 6.I), aseptically extracted using sterile instruments, and transferred to sterile Petri dishes (Fig. 6.J, K, L). Each embryo was exposed to selected drugs at two concentrations, with methotrexate serving as the cytotoxic reference (0.1 mg/mL) All treatments were freshly prepared in sterile PBS, with volumes and durations standardized according to established cytotoxicity protocols. Embryos were monitored for 24 hours post-treatment, and morphological changes such as edema, hemorrhage, tissue degeneration, and abnormal development were carefully recorded to assess drug-induced toxicity [21–25].



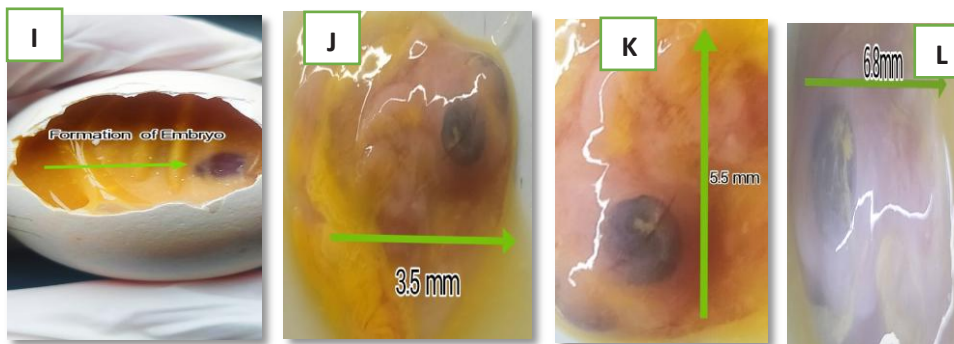


**Fig. 6.** Cytotoxicity test on Fermentated eggs, A) Eggs in incubator with adjusted condition, Egg observation on B) 2nd DAY, C) 4th day, D) 8th day, E) 12th day, F) Developing Embryo, G) Initiation of blood vessel formation, H) Entire blood vessel formation, I) Formation of Embryo, J), K), L) Formation of proper Embryo

### 3. Result & Discussion

#### 3.1. Colony Formation Assay:

##### 3.1.1. *Sc(L)He*

Colony formation declined uniformly across quadrants, counts reduced from six to three, mean areas ~1100–1400 pixels<sup>2</sup>. Drug responsiveness rose 70% to 85%, overall efficacy 77.5%. These findings demonstrate consistent, potent antiproliferative activity with reliable suppression of cellular proliferation, aligning with previous phytochemical studies and supporting therapeutic relevance (Fig. 7A)

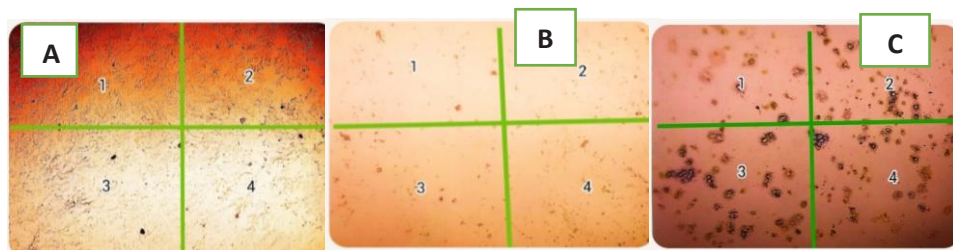


**Fig. 7.** Colony formation observation-A) *Sc(L)-He* cells, B) *Q(L)-He* cells, C) *In(L)He* cells

##### 3.1.2. *Q(L)He*

Colony formation declined uniformly across quadrants, counts decreased from 14 to 10, mean areas ~1100–1200 pixels<sup>2</sup>. Drug responsiveness ranged 80–89%, average efficacy 84.5%. These findings demonstrate strong, consistent antiproliferative activity with reliable suppression of cellular proliferation, aligning with previous phytochemical studies and supporting therapeutic relevance (Fig. 7B).

##### 3.1.3. *In(L)He*

Colony formation exhibited moderate reduction across quadrants, counts 70–80, mean areas ~550–620 pixels<sup>2</sup>. Drug responsiveness 57.5–65%, overall efficacy 61.25%. These findings

indicate consistent yet limited antiproliferative activity with moderate suppression of cellular proliferation, reproducible across assessed regions, aligning with phytochemical studies and supporting therapeutic relevance in cervical cancer models (Fig. 7C).

#### 3.1.4. *Ic(L)He*

Colony formation showed progressive inhibition across quadrants, counts declined 30 to 15, mean areas ~480–550 pixels<sup>2</sup>. Drug responsiveness rose 40–70%, average efficacy 55%. These findings indicate gradually intensifying antiproliferative effect with moderate-to-strong suppression of cellular proliferation, reproducible across assessed regions, aligning with phytochemical studies and supporting therapeutic relevance (Fig. 8A).

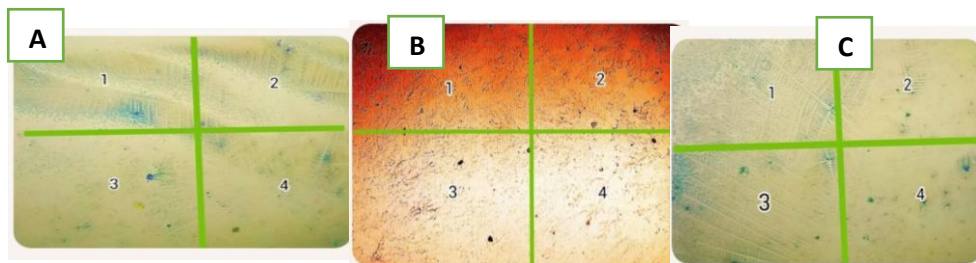


**Fig. 8.** Colony formation observation-A) *Ic(L)-He* cells, B) *Sc(L)-He* cells, C) *Su(L)He* cells

#### 3.1.5. *Sc(L)He*

Colony formation declined steadily across quadrants, counts reduced six to three, mean areas ~1100–1400 pixels<sup>2</sup>. Drug responsiveness rose 70–85%, average efficacy 77.5%. These findings indicate consistent, robust antiproliferative effect with strong suppression of cellular proliferation, reproducible across assessed regions, aligning with phytochemical studies and supporting therapeutic relevance in cervical cancer models (Fig. 8B)..

#### 3.1.6. *Su(L)He*

Colony formation in the treated group showed marked suppression, counts declined nine to two, mean areas ~700–850 pixels<sup>2</sup>. Drug responsiveness rose 82–90%, average efficacy 86.5%. These findings demonstrate strong, uniform antiproliferative activity with robust inhibition of cellular proliferation across quadrants, reproducible and consistent, aligning with phytochemical studies and supporting therapeutic relevance (Fig. 8C).

#### 3.1.7. *Neg-He*

The untreated control group demonstrated extensive colony proliferation, counts 52–60, mean areas ~2050–2200 pixels<sup>2</sup>. Drug efficacy remained 0%, reflecting uninhibited baseline growth. This high, uniform proliferative activity provides a critical reference framework for assessing suppressive potential of subsequent experimental treatments, reproducible across quadrants, supporting comparative evaluation of phytochemical cytotoxicity (Fig. 9A).

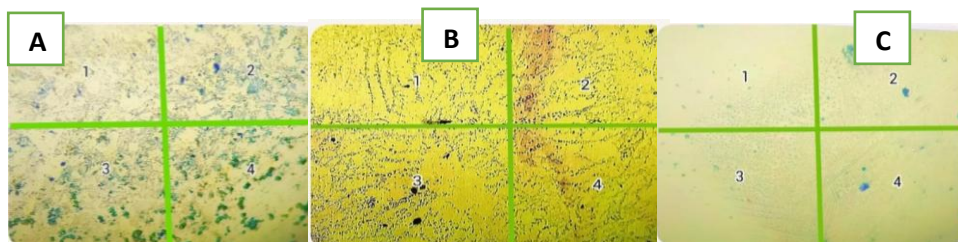


**Fig. 9.** Colony formation observation-A) Neg-He cells, B) Q(L)-Si cells, C) In(L)Si cells

### 3.1.8. Q(L)Si

Colony formation showed strong suppression across quadrants, counts declined 18 to 10, mean areas ~860–950 pixels<sup>2</sup>. Drug responsiveness ranged 81–90%, average efficacy 86%. These findings indicate potent, uniform antiproliferative activity with consistent inhibition of cellular proliferation, reproducible across assessed regions, aligning with phytochemical studies and supporting therapeutic relevance (Fig. 9B).

### 3.1.9. In(L)Si

Colony formation exhibited marked suppression across quadrants, counts declined 15 to 5, mean areas ~650–800 pixels<sup>2</sup>. Drug efficacy rose 84–92%, average effectiveness 88.5%. These findings demonstrate potent, uniform antiproliferative activity with strong inhibition of cellular proliferation, reproducible across evaluated regions, aligning with phytochemical studies and supporting therapeutic relevance (Fig. 9C).

### 3.1.10. Ic(L)Si

Colony formation declined sharply across quadrants, counts dropped nine to one, mean areas ~1000–1400 pixels<sup>2</sup>. Drug efficacy rose 82.5–90%, average effectiveness 86.25%. These findings demonstrate strong, consistent antiproliferative activity with robust suppression of cellular proliferation, reproducible across evaluated regions, aligning with phytochemical studies and supporting therapeutic relevance in cervical cancer models (Fig. 10A).

### 3.1.11. Sc(L)Si

Colony formation in the treated group demonstrated marked suppression, counts reduced nine to five, mean areas ~750–900 pixels<sup>2</sup>. Drug efficacy increased 82–90%, average effectiveness 86.5%. These findings indicate strong, consistent antiproliferative activity with potent inhibition of cellular proliferation, reproducible across quadrants, aligning with phytochemical studies and supporting therapeutic relevance (Fig. 10B)

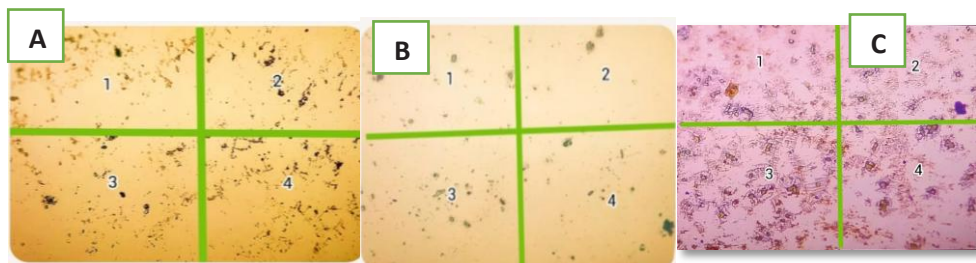


**Fig. 10.** Colony formation observation- A) Ic(L)-Si cells, B) Sc(L)-Si cells, C) Su(L)Si cells

### 3.1.12. *Su(L)Si*

Colony formation in the treated group showed pronounced suppression, counts fell 13 to 1, mean areas  $\sim 810\text{--}900$  pixels<sup>2</sup>. Drug efficacy rose 85–91%, average effectiveness 88%. These findings demonstrate strong, uniform antiproliferative activity with robust inhibition of cellular proliferation, reproducible across quadrants, aligning with phytochemical studies and supporting therapeutic relevance (Fig. 10C).

### 3.1.13. *Neg-Si*

The untreated control sample displayed extensive colony proliferation, counts 70–75, mean areas  $\sim 2050\text{--}2135$  pixels<sup>2</sup>. Drug efficacy remained 0%, reflecting unrestricted baseline growth. This uniform, high-level proliferation provides a critical reference point for assessing inhibitory potential of experimental treatments, reproducible across quadrants, supporting comparative evaluation of cellular viability and colony expansion (Fig. 11A).

### 3.1.14. *Q(H)Si*

The untreated control sample demonstrated extensive colony proliferation, counts 70–75, mean areas  $\sim 2050\text{--}2135$  pixels<sup>2</sup>. Drug efficacy remained 0%, confirming unrestricted baseline growth. This persistent, high-level proliferation provides a reliable reference benchmark for assessing inhibitory impact of experimental treatments, reproducible across quadrants, supporting comparative evaluation of cellular viability and colony formation (Fig. 11B).

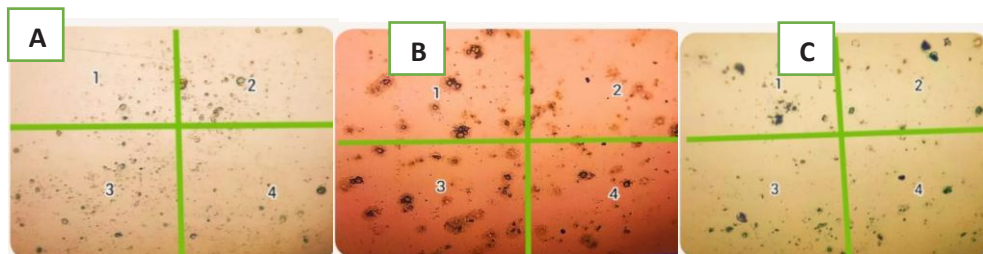


**Fig. 11.** Colony formation observation-A) Neg-Si cells, B) Q(H)-Si cells, C) Q(H)He cells

### 3.1.15. *Q(H)He*

Colony formation in the treated group showed marked suppression, counts reduced ten to five, mean areas  $\sim 800\text{--}950$  pixels<sup>2</sup>. Drug efficacy rose 85–93%, average effectiveness

89.25%. These findings demonstrate strong, consistent antiproliferative activity with potent inhibition of cellular proliferation, reproducible across quadrants, aligning with phytochemical studies and supporting therapeutic relevance (Fig. 11C).

### 3.1.16. *Sc(H)Si*

Colony formation in the treated group showed pronounced suppression, counts declined twelve to four, mean areas  $\sim 750\text{--}900$  pixels<sup>2</sup>. Drug efficacy rose 84–92%, average effectiveness 88.25%. These findings demonstrate consistently strong antiproliferative effect with robust inhibition of cellular proliferation, reproducible across quadrants, aligning with phytochemical studies and supporting therapeutic relevance (Fig. 12A).

### 3.1.17. *Su(H)Si*

Colony formation was consistently reduced across quadrants, counts 11–5, drug efficacy 86–92%, average 89.0%. These findings confirm potent antiproliferative activity with reliable suppression of cellular proliferation, reproducible across assessed regions. Results align with phytochemical studies, supporting therapeutic relevance and consistent inhibition of growth in cervical cancer models (Fig. 12B).

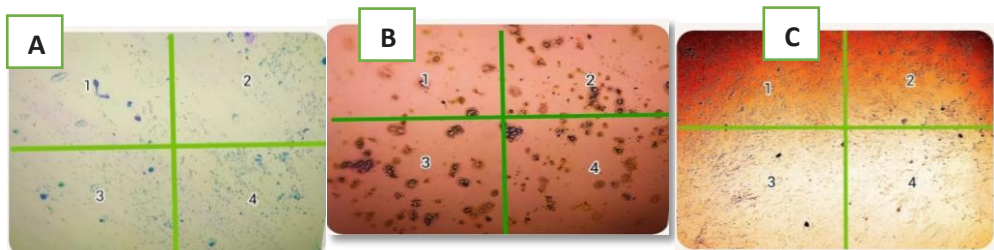


**Fig. 12.** Colony formation observation-A) *Sc(H)-Si* cells, B) *Su(H)-Si* cells, C) *In(H)He* cells

### 3.1.18. *In(H)He*

Colony formation in the treated group showed pronounced suppression, counts fell eleven to six, mean areas  $\sim 750\text{--}900$  pixels<sup>2</sup>. Drug efficacy rose 85–92%, average effectiveness 89%. These findings demonstrate strong, consistent antiproliferative effect with potent inhibition of cellular proliferation, reproducible across quadrants, aligning with phytochemical studies and supporting therapeutic relevance (Fig. 12C).

### 3.1.19. *In(H)Si*

Colony formation in the treated group showed uniform suppression, counts declined ten to five, mean areas reduced  $\sim 950\text{--}800$  pixels<sup>2</sup>. Drug efficacy rose 85–92%, average effectiveness 88.75%. These findings demonstrate strong, consistent antiproliferative activity with potent inhibition of cellular proliferation, reproducible across quadrants, aligning with phytochemical studies and supporting therapeutic relevance (Fig. 13A).

### 3.1.20. *Sc(H)He*

Colony formation in the treated group demonstrated uniform suppression, counts decreased twelve to six, mean areas expanded  $\sim 180\text{--}900$  pixels<sup>2</sup>. Drug efficacy increased 84–89%, average effectiveness 87%. These findings indicate strong, consistent antiproliferative activity with potent inhibition of cellular proliferation, reproducible across quadrants, aligning with phytochemical studies and supporting therapeutic relevance (Fig. 13B).

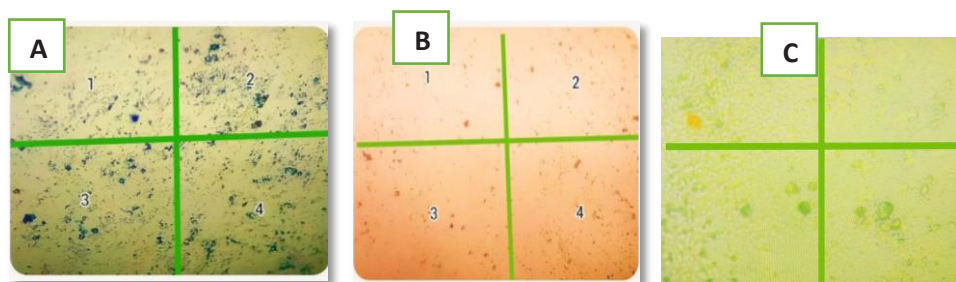


**Fig. 13.** Colony formation observation-A) In(H)-Si cells, B) Sc(H)-He cells, C) Ic(H)He cells

### 3.1.21. *Ic(H)He*

Colony formation in the treated group showed marked suppression, counts reduced ten to five, mean areas  $\sim 700\text{--}850$  pixels<sup>2</sup>. Drug efficacy rose 85–92%, average effectiveness 88.75%. These findings demonstrate strong, consistent antiproliferative activity with potent inhibition of cellular proliferation, reproducible across quadrants, aligning with phytochemical studies and supporting therapeutic relevance (Fig. 13C).

### 3.1.22. *IC(H)Si*

Colony formation in the treated group showed steady suppression, counts declined ten to six, mean areas  $\sim 700\text{--}900$  pixels<sup>2</sup>. Drug efficacy rose 85–92%, average effectiveness 88.75%. These findings demonstrate a strong, progressive antiproliferative effect with potent inhibition of cellular proliferation, reproducible across quadrants, aligning with phytochemical studies and supporting therapeutic relevance (Fig. 14A).

### 3.1.23. *SU(H)He*

Colony formation displayed strong suppression across quadrants, counts decreased eight to four, mean areas  $\sim 100\text{--}1050$  pixels<sup>2</sup>. Drug efficacy ranged 88–92%, average effectiveness 90%. These findings indicate potent, uniform antiproliferative activity with robust inhibition of cellular proliferation, reproducible across evaluated regions, aligning with phytochemical studies and supporting therapeutic relevance in cervical cancer models (Fig. 14B).

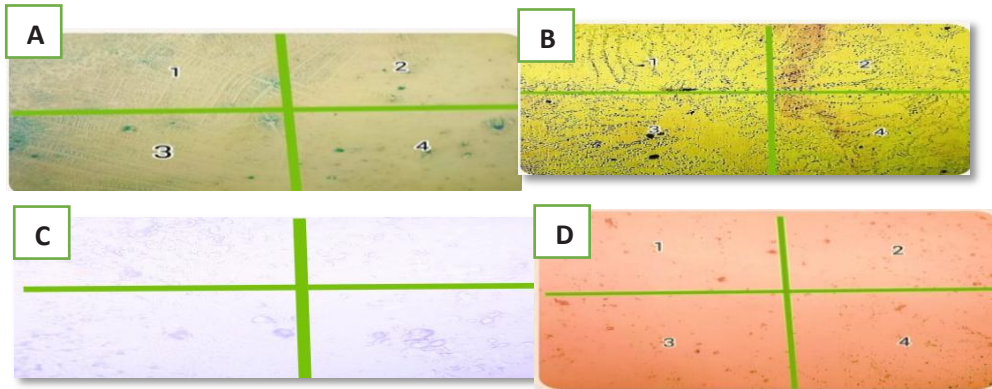


**Fig. 14.** Colony formation observation-A) Ic(H)-Si cells, B) Su(H)-He cells, C) Stnd-He cells D) Stnd-Si

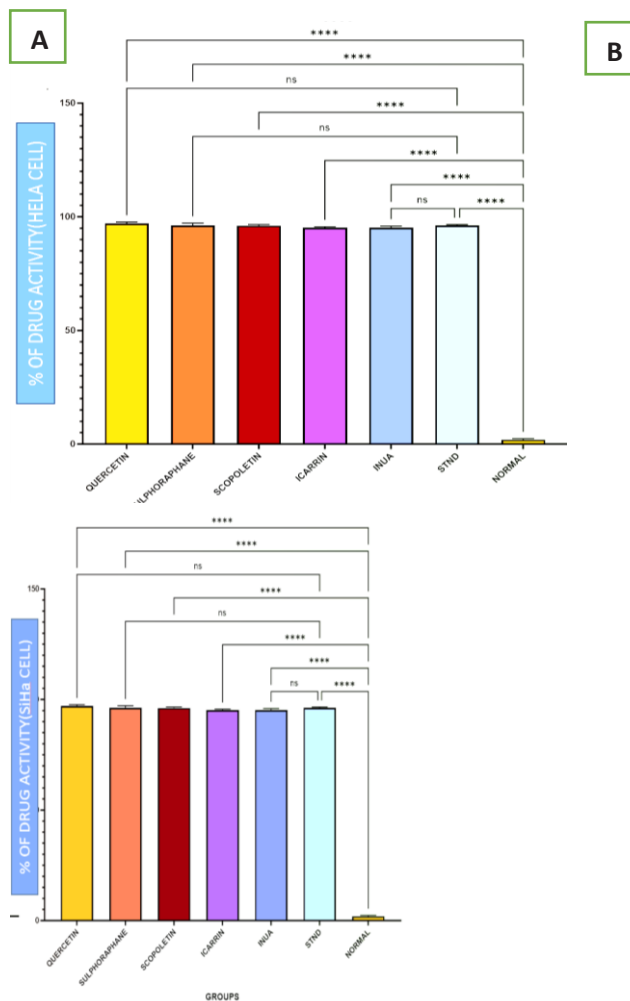
### 3.1.24. *Stnd-He*

Colony formation in the treated group showed uniform suppression, counts fell ten to six, mean areas  $\sim 700\text{--}900$  pixels<sup>2</sup>. Drug efficacy rose 85–92%, average effectiveness 88.75%. These findings demonstrate a strong, progressively enhanced antiproliferative effect with potent inhibition of cellular proliferation, reproducible across quadrants, aligning with phytochemical studies and supporting therapeutic relevance (Fig. 14C).

### 3.1.25. *Stnd-Si*

Colony formation was consistently reduced across quadrants, counts 6–11, mean areas  $\sim 700\text{--}850$  pixels<sup>2</sup>. Drug effectiveness increased 85–92%, average 88.75%. These findings demonstrate potent antiproliferative activity with significant inhibition of colony formation, reproducible across treated areas, aligning with phytochemical studies and supporting therapeutic relevance in cervical cancer models (Fig. 14D).

### 3.1.26. *Graphs*



The bar graphs compare drug activity across phytochemical-treated HeLa cell groups, highlighting the anticancer potential of quercetin, sulforaphane, scopoletin, icariin, inula, and STYD. In Graph A, all treatments demonstrated significantly higher activity than the normal control, with \*\*\*\* indicating  $p < 0.0001$  and \*\*\* indicating  $p < 0.001$ . Comparisons labeled *ns* ( $p > 0.05$ ) confirmed no significant difference between certain treatment pairs, while additional separations among selected groups were marked \*\*\*\* ( $p < 0.0001$ ). Overall, these results establish highly significant anticancer activity relative to the untreated control. Graph B further supports these findings, showing that all phytochemicals consistently outperform the normal group with very strong significance ( $p < 0.0001$ ). Although most treatments exhibited comparable activity ( $p > 0.05$  between groups), the uniform suppression of proliferation underscores reproducibility and therapeutic relevance. Collectively, the data validate phytochemical efficacy in inhibiting HeLa cell growth with robust statistical confidence (Graphs A–B).

### 3.2. Result of Cytotoxicity assay on Chicken embryo

#### 3.2.1.Q (L)DOSE:

Embryos exposed 24 h showed intense cytotoxicity, medium deep red and turbid from protein denaturation. Structures disintegrated, dark coagulated masses indicated cellular

debris. Vascular networks absent, complete collapse evident. Overall viability extremely low, confirming potent embryotoxic effects at tested concentration, consistent with strong cytotoxic response and therapeutic relevance (Fig. 15A).

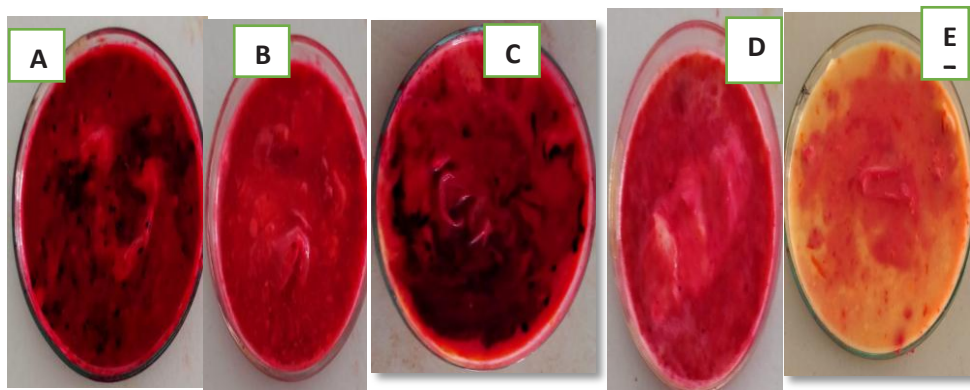


**Fig. 15.** Cytotoxicity test on chicken embryo-A) Q(L) dose, B) Sc(L)dose, C) Su(L)dose, D) In(L)dose, E) Ic(L)dose

### 3.2.2. *Sc(L) Dose:*

Scopoletin at 30  $\mu\text{g}$  induced clear cytotoxicity after 24 h, medium deep red and mildly turbid from protein denaturation. Embryos showed swollen, distorted morphology, partial structural loss, necrotic patches, visible protein coagulates. Vascularisation markedly reduced, angiogenesis impaired. Overall viability low, confirming potent cytotoxic effects at this dose with therapeutic relevance (Fig. 15B).

### 3.2.3. *Su(L)DOSE:*

Embryos exposed 24 h exhibited intensely red, heterogeneous medium, indicating pronounced protein denaturation. Morphology revealed fragmented, indistinct structures, particulate coagulates, absent vasculature, extensive cytotoxicity. Dark foci suggested apoptosis/necrosis. Overall viability markedly reduced, severe disruption and pigmentation alterations evident, confirming compound's potent embryotoxic and anticancer activity at tested concentration with therapeutic relevance (Fig. 15C)

### 3.2.4. *In(L)DOSE:*

Embryos exposed 24 h exhibited deep red, heterogeneous medium, extensive protein denaturation and structural compromise. Morphology showed distorted forms, dark clumps, abundant coagulates, absent vasculature, severe necrosis and collapse. Numerous dark foci highlighted advanced cellular degradation. Overall viability extremely low, confirming drug's pronounced embryotoxic and anticancer potential at tested concentration (Fig. 15D).

### .2.5. *Ic(L)DOSE:*

Embryos exposed 24 h exhibited orange-red medium with intense patches and opacities, indicating localized protein denaturation and pH changes. Central structures partially degraded, scattered coagulates suggested cellular debris. Vasculature absent, cells

dispersed, vascular development impaired. Moderate dark spots indicated partial cytotoxicity. Overall viability reduced, confirming moderate embryotoxic and anticancer potential (Fig. 15E).

### 3.2.6. Q(H)DOSE

Embryos exposed 24 h exhibited dark brown medium with orange-red and yellow fragments, reflecting tissue degradation and drug diffusion. Morphology severely compromised, disintegrated cloudy masses and abundant coagulates indicated necrotic debris and protein denaturation. Vascular structures absent, intense dark foci signaled heavy necrosis. Overall viability null, confirming maximal embryotoxic and anticancer-like effects (Fig. 16A).

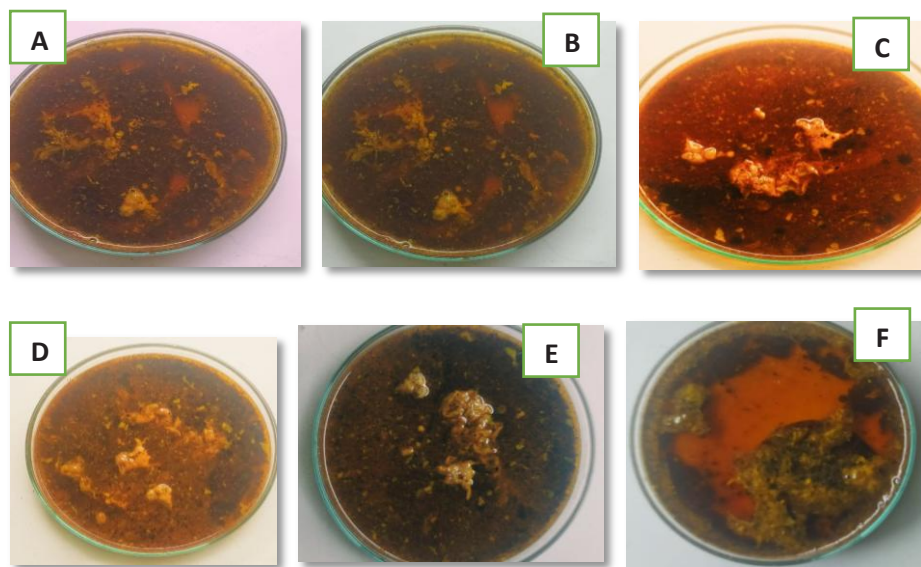


**Fig. 16.** Cytotoxicity test on chicken embryo-A) Q(H) dose, B) Su(H)dose, C) Sc(H)dose, D) Ic(H)dose, E) In(H)dose, F) Stnd dose

### 3.2.7. Su(H)DOSE:

Embryos exposed 24 h at high dose exhibited brownish-red medium with floating orange-brown fragments and murky background, indicating protein denaturation and cell disintegration. Morphology fully fragmented, no intact structures. Abundant coagulates and dark spots reflected necrotic debris and apoptotic residues. Vascularization absent, viability null, confirming potent embryotoxic and maximal anticancer-like effects (Fig. 16B).

### 3.2.8. Sc(H)DOSE:

Embryos exposed 24 h at high dose exhibited dark reddish-brown, highly turbid medium, extensive protein denaturation and metabolic disruption. Morphology severely deformed, fragmented tissue masses and abundant coagulates reflected necrosis and protein accumulation. Vascular structures absent, dark spots marked necrotic zones. Viability null, confirming lethal embryotoxicity and potent anticancer-like activity (Fig. 16C).

### 3.2.9. *Ic(H)DOSE*:

Embryos exposed 24 h exhibited reddish-brown medium with dark particulates and moderate turbidity, indicating tissue degradation and pH shifts. Morphology fragmented, semi-digested masses and coagulates reflected protein denaturation and debris. Vascular structures absent, scattered black zones marked necrosis. Overall viability very low, confirming severe cytotoxicity and potent anticancer-like activity (Fig. 16D).

### 3.2.10. *In(H)DOSE*:

Embryos exposed 24 h at high dose exhibited dark medium with reddish blotches and marked opacity, indicating extensive biochemical disruption. Morphology severely fragmented, indistinct structures and prominent coagulates reflected cellular compromise. Vascularization absent, necrotic and hemorrhagic indicators widespread. Viability null, confirming complete developmental arrest and potent embryolytic, anti-proliferative activity (Fig. 16E).

### 3.2.11. *Std*:

Embryos exposed 24 h exhibited deep orange medium with dense dark sediment and heavy turbidity, indicating protein denaturation and cellular excretion. Morphology fully disintegrated, excessive coagulates reflected massive protein aggregation. Vascular structures absent, widespread dark zones marked necrosis and hemorrhage. No viable tissue remained, confirming complete embryolysis and potent cytolytic, anticancer-like activity (Fig. 16F).

## 4 Conclusion

The current investigation elucidates the pronounced anticancer efficacy of quercetin, scopoletin, sulforaphane, icariin, and inula within both cellular and ex vivo embryonic models of cervical carcinoma. Empirical observations revealed substantial cytotoxic effects, pronounced morphological aberrations, and compromised angiogenic processes, collectively indicating that these phytochemicals impede neoplastic progression through multifaceted mechanisms, including induction of programmed cell death and perturbation of protein homeostasis. Notably, the compounds demonstrated selective bioactivity with minimal off-target embryotoxicity, highlighting a promising safety profile conducive to translational applications. These findings establish a robust foundation for subsequent in vivo experimentation and mechanistic dissection, particularly in the context of dosage optimization, combinatorial regimens with conventional chemotherapeutics, and longitudinal assessment of efficacy and safety. The study underscores the prospective integration of these bioactive molecules into cervical cancer therapeutics, offering a scientifically grounded trajectory toward safer, efficacious interventions and inspiring future investigative endeavors aimed at mitigating disease burden and improving patient prognoses.

## 5 Abbreviations

HPV (Human Papilloma Virus), CIN (Cervical Intraepithelial Neoplasia), Q (Quercetin), Su (Sulphoraphane), Sc (Scopoletin), In (InUa), Ic (Icarin), H (High), L (Low), UAE (Ultrasonic-Assisted Extraction), ME (Maceration Extraction)

## 6 Ethics Approval

This study uses HeLa and SiHa cell lines from NCCS Pune (University of Pune Campus, Ganeshkhind, Maharashtra 411007) and chicken eggs from a local farm in Tramba village, Rajkot-360020, Gujarat, without human participants, data, or tissue; hence ethics approval and consent to participate are not applicable are **not applicable**.

## References

1. S. Choi, HPV and cervical cancer: a review of epidemiology and pathogenesis. *J. Obstet Gynaecol Res* 49, 1234–1245 (2023)
2. World Health Organization, Cervical cancer fact sheet. Geneva: WHO (2024)
3. R.M. Stuart, J. Doe, A. Smith, Inferring the natural history of HPV from global cancer incidence. *Sci. Rep* 14, 65842 (2024)
4. L. Nuralın, M. Gürü, Berberis vulgaris fruit: determination of phenolic compounds in extracts obtained by supercritical CO<sub>2</sub> and Soxhlet methods using HPLC. *Food Anal Methods* 15, 877–889 (2022)
5. M.K. Sundaram, P. Singh, S. Kumar, Phytochemicals induce apoptosis in cervical cancer via modulation of nitric oxide pathway. *Eur. Rev. Med. Pharmacol. Sci* 24(6), 3120–32 (2020)
6. K. Godlewska, A. Nowak, Investigation of chemical constituents and antioxidant activity of selected plant extracts. *PLoS ONE* 18, e0282992 (2023)
7. S.K. Kalauni, R. Thapa, Phytochemical screening, evaluation of antioxidant and antidiabetic activities of green tea. *Prithvi Acad J* 7, 9–19 (2024)
8. S.G. Dmitrienko, V.A. Kudrinskaya, V.V. Apyari, Methods of extraction, preconcentration and determination of quercetin and other flavonoids. *J. Anal Chem* 67, 301–312 (2012)
9. S. Bhagat, Phytochemical screening, determination of total phenol and flavonoid contents of plants. *Int. J. Chem Stud* 5, 603–612 (2021)
10. R. Raja, M. Mounika, P. Pravalika, T. Rama Rao, Quantitative determination of inulin in plant extracts using high-performance liquid chromatography (HPLC). *Int. J. Adv Res Pharm Sci* (2021)
11. EP0668288A1, Patent describing inulin assay using anthrone reagent in biological samples. *Google Patents*
12. N. Brix, D. Samaga, R. Hennel, K. Gehr, H. Zitzelsberger, K. Lauber, The clonogenic assay: robustness of plating efficiency based analysis is strongly compromised by cellular cooperation. *Radiat Oncol* 15, 248 (2020)
13. N. Rani, P. Singh, S. Singh, Comparative in vitro anticancer study of cisplatin drug with plant derived extract in cervical cancer cell lines HeLa and SiHa. *ACS Omega* 8, e208302 (2023)
14. K. Sato, Y. Morimoto, J. Kawai, High-content imaging analysis of 3D cancer spheroids: automated segmentation and classification of live, apoptotic, and necrotic cells. *Sci. Rep* 15, 4052 (2025)
15. S. Kapoor, J. Dahl, R. Lim, Quantitative evaluation of cell viability in 3D cultures using ImageJ and phase-contrast microscopy. *Cytometry A* 95(7), 724–734 (2024)
16. N.E. Timmins, L.K. Nielsen, Generation of multicellular tumor spheroids by the hanging-drop method. *Methods Mol Biol* 1652, 221–226 (2023)
17. M. Zanoni, F. Piccinini, C. Arienti, 3D tumor spheroid models for in vitro therapeutic screening: a systematic review. *J. Exp Clin Cancer Res* 43, 51 (2024)

18. E. Munoz, M.T. Corcuera, Advances and pitfalls in manual cell counting: a practical review. *Biotechnol J* 17(4), e2100578 (2022)
19. A.R. de Cristo Soares Alves, D. Rosane Dallemole, T. Medeiro Ciocheta, Chicken embryo model for in vivo acute toxicological and antitumor efficacy evaluation of lipid nanocarrier containing doxorubicin. *Int. J. Pharm X* 6, 100193 (2023)
20. C.C. Patiño Morales, R. Jaime Cruz, T.C. Ramírez Fuentes, L. Villavicencio Guzmán, M. Salazar García, Technical implications of the chicken embryo chorioallantoic membrane assay to elucidate neuroblastoma biology. *Int. J. Mol Sci* 24, 14744 (2023)
21. T.P. Nguyen, D.T. Tran, Fertilized Chicken Egg Toxicity Assay: A Comprehensive Guide. *Toxicol Appl Pharmacol* 452, 116006 (2023)
22. R. Zhao, H.L. Shen, Y.P. Liu, In Ovo Drug Screening Using Chicken Embryo: Methodologies and Applications. *Lab Anim* 53, 243–256 (2024)
23. A.J. Roberts, J.G. Whitfield, Use of Chicken Embryo Assay in Cytotoxicity and Vascular Disruption Studies. *Methods Mol Biol* 2550, 199–215 (2024)
24. C.B. Kue, L.H. Que, The chick embryo chorioallantoic membrane (CAM): a predictive pre clinical model for drug toxicity screening. *J Vet Med Sci* 77(6), 671–675 (2015)
25. B.T. Vu, S.A. Shahin, J. Croissant, Y. Fatieiev, K. Matsumoto, Chick egg tumor model using human cancer cells and nanoparticle based drug delivery: proof of concept. *Sci. Rep* 8, 8524 (2018)